催 化 学 报
2011 Chinese Journal of Catalysis Vol. 32 No. 5

文章编号: 0253-9837(2011)05-0727-09 国际版 DOI: 10.1016/S1872-2067(10)60220-3 研究论文: 727~735

CeO_2添加对Ag/Al_2O_3催化剂低温氨氧化性能的影响

张 丽, 刘福东[a], 余运波, 刘永春, 张长斌, 贺 泓[b]

中国科学院生态环境研究中心, 环境化学与生态毒理学国家重点实验室, 北京 100085

摘要: 采用活性测试和氮气吸附、X射线衍射、X射线光电子能谱、紫外-可见漫反射吸收光谱、高倍透射电镜、原位漫反射傅里叶变换红外光谱和O_2脉冲吸附等研究了铈添加对Ag/Al_2O_3催化剂低温氨氧化性能的影响. 结果表明, 适量铈的添加可以明显促进Ag/Al_2O_3催化剂的低温氨氧化活性, 且对催化剂的选择性影响不大. 添加铈不仅可以促进Ag/Al_2O_3催化剂表面吸附和活化O_2的能力, 而且可促进催化剂表面对氨的解离吸附和活化. 这是铈促进Ag/Al_2O_3催化剂低温氨氧化活性的主要原因.

关键词: 氨; 银; 铈; 氧化铝; 负载型催化剂; 氧气吸附; 高倍透射电镜; 原位漫反射傅里叶变换红外光谱

中图分类号: O643 **文献标识码:** A

收稿日期: 2011-01-04. 接受日期: 2011-02-23.

[a]通讯联系人. 电话/传真: (010)62911040; 电子信箱: fdliu@rcees.ac.cn

[b]通讯联系人. 电话/传真: (010)62849123; 电子信箱: honghe@rcees.ac.cn

基金来源: 国家重点基础研究发展计划 (973 计划, 2010CB732304); 国家高技术研究发展计划 (863 计划 2009AA064802); 国家自然科学基金委员会创新研究群体科学基金 (50921064).

本文的英文电子版(国际版)由Elsevier出版社在ScienceDirect上出版(http://www.sciencedirect.com/science/journal/18722067).

Effects of Adding CeO_2 to Ag/Al_2O_3 Catalyst for Ammonia Oxidation at Low Temperatures

ZHANG Li, LIU Fudong[a], YU Yunbo, LIU Yongchun, ZHANG Changbin, HE Hong[b]

State Key Laboratory of Environmental Chemistry and Ecotoxicology, Research Center for Eco-Environmental Sciences, Chinese Academy of Sciences, Beijing 100085, China

Abstract: The effects of adding CeO_2 to Ag/Al_2O_3 on the selective catalytic oxidation of ammonia to nitrogen were investigated by activity test and N_2 physisorption, X-ray diffraction, X-ray photoelectron spectroscopy, UV-Vis diffuse-reflectance spectroscopy, high resolution transmission electron microscopy, in situ diffuse reflectance infrared Fourier transform spectroscopy of NH_3 adsorption, and O_2-pulse adsorption. Adding a suitable amount of CeO_2 improved the catalytic activity of Ag/Al_2O_3 for NH_3 oxidation at temperatures below 160 ^oC, and slightly influenced N_2 selectivity by improving the catalyst's ability to adsorb and activate O_2 and the adsorption and activation of NH_3.

Key words: ammonia; silver; cerium; alumina oxide; supported catalyst; oxygen uptake; high resolution transmission electron microscopy; in situ diffuse reflectance infrared Fourier transform spectroscopy

Received 4 January 2011. Accepted 23 February 2011.

[a]Corresponding author. Tel/Fax: +86-10-62911040; E-mail: fdliu@rcees.ac.cn

[b]Corresponding author. Tel/Fax: +86-10-62849123; E-mail: honghe@rcees.ac.cn

This work was supported by the National Basic Research Program of China (973 Program, 2010CB732304), the National High Technology Research and Development Program of China (863 Program, 2009AA064802), and the National Natural Science Foundation of China (50921064).

English edition available online at Elsevier ScienceDirect (http://www.sciencedirect.com/science/journal/18722067).

The selective catalytic oxidation (SCO) of NH_3 to nitrogen (N_2) and water can reduce NH_3 emissions from chemical processes such as the selective catalytic reduction (SCR) of NO_x by NH_3 and from soda production [1–5]. In particu-

lar, the low temperature oxidation of NH_3 to N_2 has important environmental applications. Noble metals such as Pt and Ir are the most active but least selective [5–7]. Gang et al. [6,8] reported that an alumina-supported Ag (10 wt% Ag/Al_2O_3) catalyst was extremely active for NH_3 oxidation at low temperatures, and was superior to the noble metals. Nonetheless, there is still a considerable need for better catalysts that are active at low temperatures. The addition of CeO_2 improves the NH_3 oxidation activities of Au-, Cu-, and Ag-based catalysts [2,3]. Lippits et al. [3] found that adding CeO_x to Ag-based catalyst lowered the temperature for the onset of oxidation from 300 to 200 °C. However, the role of CeO_2 in the Ag-based catalyst has not been studied in detail. Recently, we investigated the SCO of NH_3 over a 10 wt% Ag/Al_2O_3 catalyst and discovered that the Ag valence state and particle size were significant for activity and N_2 selectivity at low temperatures [7]. To further improve the catalytic performance at low temperatures, we investigated the catalytic effects and the role of CeO_2 addition on Ag/Al_2O_3 for the oxidation of NH_3.

1 Experimental

1.1 Catalyst preparation and H_2-pretreatment

The $Ag\text{-}Ce/Al_2O_3$ catalysts used had different Ce loadings and were prepared by co-impregnating $\gamma\text{-}Al_2O_3$ powder (250 m^2/g) with appropriate amounts of $AgNO_3$ and $Ce(NO_3)_3{\cdot}6H_2O$ in aqueous solution. After impregnation, excess water was removed in a rotary evaporator at 80 °C and the samples were dried overnight at 120 °C before calcination at 600 °C in air for 3 h. The mass ratio of Ag to $\gamma\text{-}Al_2O_3$ was maintained at 0.1 and the resulting $Ag\text{-}Ce/Al_2O_3$ samples were designated as $Ag_{0.1}Ce_y/Al_2O_3$, where y was the Ce/Al_2O_3 mass ratio. The catalysts were sieved to a particle size of 20–40 mesh and pretreated in a H_2/N_2 flow (20 vol% H_2, 60 cm^3/min) at 400 °C for 2 h before testing.

1.2 Activity test

1.2.1 Steady state activity for NH_3 oxidation

The SCO activity was measured in a fixed-bed quartz reactor using 0.2 g catalyst. The reactant gas was obtained from blends of different gas flows at a combined flow rate of 200 cm^3/min (W/F = 0.06 (g·s)/cm^3). A typical reactant gas composition was 0.05 vol% NH_3 and 10 vol% O_2, with N_2 providing the balance. The individual NH_3, O_2, and N_2 flow rates were controlled by mass flow controllers. Inlet and outlet gas compositions were analyzed using an online NEXUS 670-FTIR spectrometer fitted with a 200 cm^3 gas cell. N_2 balance was calculated using M_{NH3} (inlet) = M_{NH3} (outlet) + $2M_{N2O}$ + M_{NOx} + $2M_{N2}$. These operating conditions were used as the standard.

1.2.2 Evolution of NH_3 oxidation with time at various temperatures

A H_2-pretreated $Ag_{0.1}Ce_{0.1}/Al_2O_3$ catalyst was fed with the reactant mixture and kept at temperatures of 100 and 160 °C, respectively, to evaluate the activity of the catalyst under these different conditions. The evolution of NH_3 oxidation versus time was recorded at both 100 and 160 °C.

1.3 Characterization of catalyst

N_2 adsorption-desorption isotherms were obtained by the adsorption of N_2 at –196 °C using a Quantasorb-18 automatic instrument (Autosorb-1C, Quanta Chrome Instrument, USA). Specific areas were computed from these isotherms by the Brunauer-Emmett-Teller (BET) method. The pore size distribution was calculated using the Barrett-Joiner-Halenda (BJH) method. Before measurement, samples were degassed at 300 °C for 4 h.

Powder X-ray diffraction (XRD) scans of the catalysts were conducted in the 2θ range of 20° to 70° at a scan speed of 6°/min using a Rigaku D/max-RB X-ray diffractometer (Japan) with Cu K_α radiation, operating at 40 kV and 40 mA.

The surface structure and concentration of the active species on the catalysts were characterized by X-ray photoelectron spectroscopy (XPS). Spectra were recorded using a PHI Quantera spectrometer (ULVAC-PHI, Inc. USA) with Al K_α radiation ($h\nu$ = 1486.7 eV). The binding energies were calibrated against the C 1*s* peak of C present as a contaminant on the catalyst (284.8 eV).

UV-Vis diffuse-reflectance spectra (UV-Vis DRS) were recorded under ambient conditions using a U-3010 (Hitachi, Japan) spectrometer with a standard diffuse reflectance unit. The scan range was 190–850 nm and the scan rate was 300 nm/min. The measured spectra were treated by Kubelka-Munk functions and deconvoluted into Gaussian peaks that were used for the quantitative assignment of different Ag and Ce species [9–18].

High-resolution transmission electron microscopy (HR-TEM) images were recorded on an H-800 (Hitachi, Japan) instrument. The accelerating voltage for the microscope was 200 kV, the point resolution was 0.204 nm, and 200–300 particles were counted to evaluate the particle size (diameter) distribution.

In situ diffuse reflectance infrared Fourier transform spectra (in situ DRIFTS) were recorded using a Nexus 670 (Thermo Nicolet) FT-IR spectrometer equipped with an in

situ diffuse reflection chamber and a high sensitivity mercury-cadmium-telluride (MCT) detector. A sample of ca. 30 mg was ground finely and placed into a ceramic crucible. A feed gas mixture, controlled by mass flow meters, was supplied at a flow rate of 100 cm^3/min. The samples were first treated in a flow of high purity 10 vol% O_2/N_2 at 500 °C for 0.5 h and then cooled to room temperature, followed by H_2-pretreatment in a flow of H_2/N_2 (20 vol% H_2) at 400 °C for 1 h before being cooled to the desired temperature in a flow of high purity N_2. At each temperature, the background spectrum was recorded in flowing N_2, and it was subtracted from the sample spectrum obtained at the same temperature. All spectra were recorded at a resolution of 4 cm^{-1} with 100 accumulated scans.

O_2 uptake was determined by O_2-pulse adsorption at various temperatures over H_2-pretreated $Ag_{0.1}/Al_2O_3$, $Ce_{0.1}/Al_2O_3$, and $Ag_{0.1}Ce_{0.1}/Al_2O_3$ catalysts using a Quantasorb-18 automatic instrument (Quanta Chrome Instrument Co, USA). Prior to the O_2-pulse adsorption, 300 mg sample was reduced in situ with a flow of 5 vol% H_2/Ar (40 cm^3/min, 10 °C/min) at 400 °C for 2 h. Then He gas (40 cm^3/min) was passed over the sample for 1.5 h. After cooling to the desired temperature in He, O_2 pulses (4.46 μmol) were injected into a He carrier flowing over the sample. The time intervals between the O_2 pulses were about 100 s. The O_2 signal was analyzed online with an Autosorb-1-C TCD controller.

2 Results and discussion

2.1 NH_3 oxidation over different $Ag_{0.1}Ce_y/Al_2O_3$ catalysts

After similar pretreatment, the catalysts (200 mg) were tested under standard conditions for their activities. The activities of the $Ag_{0.1}Ce_y/Al_2O_3$ catalysts with different Ce/Al_2O_3 mass ratios are illustrated in Fig. 1. The NH_3 conversion over Ce-promoted Ag/Al_2O_3 catalysts at low temperature was increased comparing with unpromoted $Ag_{0.1}/Al_2O_3$. However, although increasing the mass ratio to 0.1 enhanced NH_3 oxidation to the highest conversion, further increase of this ratio gave lower NH_3 conversion. This indicated that adding CeO_2 to Ag/Al_2O_3 improved the catalytic activity of Ag/Al_2O_3 at temperatures below 160 °C, and the best Ce/Al_2O_3 mass ratio was 0.1. The conversion of NH_3 using the $Ag_{0.1}Ce_{0.1}/Al_2O_3$ catalyst at 100 °C was 73%, which was significantly higher than the 30% obtained with unpromoted $Ag_{0.1}/Al_2O_3$ catalyst under standard conditions.

The effects of H_2-pretreatment and the effects of CeO_2 on NH_3 oxidation at low temperatures over the $Ag_{0.1}Ce_{0.1}/Al_2O_3$ catalyst were also investigated (results not shown here) by comparing the activities of H_2-pretreated $Ag_{0.1}Ce_{0.1}/Al_2O_3$, $Ce_{0.1}/Al_2O_3$, and fresh $Ag_{0.1}Ce_{0.1}/Al_2O_3$ catalysts. Both the fresh $Ag_{0.1}Ce_{0.1}/Al_2O_3$ and H_2-pretreated $Ce_{0.1}/Al_2O_3$ catalysts showed little or no activity below 160 °C, while high NH_3 conversion occurred with the H_2-pretreated $Ag_{0.1}Ce_{0.1}/Al_2O_3$ catalyst at temperatures below 160 °C. Clearly, H_2-pretreatment enhanced significantly the low temperature activity of $Ag_{0.1}Ce_{0.1}/Al_2O_3$, although $Ce_{0.1}/Al_2O_3$ was inactive at low temperatures (≤160 °C). The stability of H_2-pretreated $Ag_{0.1}Ce_{0.1}/Al_2O_3$ for NH_3 oxidation was evaluated at 100 and 160 °C. The results are shown in Fig. 2. NH_3 conversion at 100 °C decreased gradually over 48 h from 73% to 37%, while the 100% NH_3 conversion at 160 °C continued for more than 96 h.

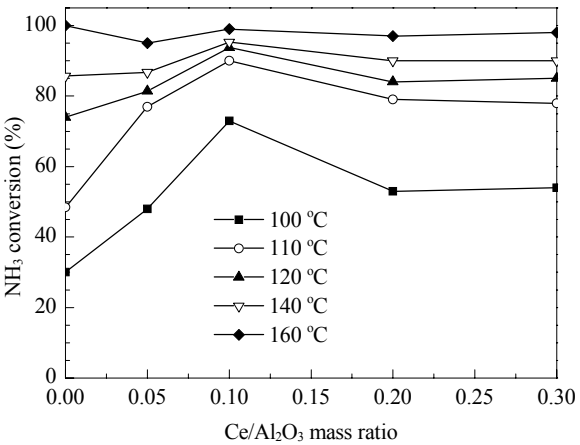

Fig. 1. Catalytic performance of the H_2-pretreated $Ag_{0.1}Ce_yAl_2O_3$ catalysts with different Ce/Al_2O_3 mass ratios for NH_3 oxidation at different temperatures. Reaction conditions: NH_3 0.05 vol%, O_2 10 vol%, N_2 as balance, flow rate 200 cm^3/min, catalyst 0.2 g (W/F = 0.06 (g·s)/cm^3).

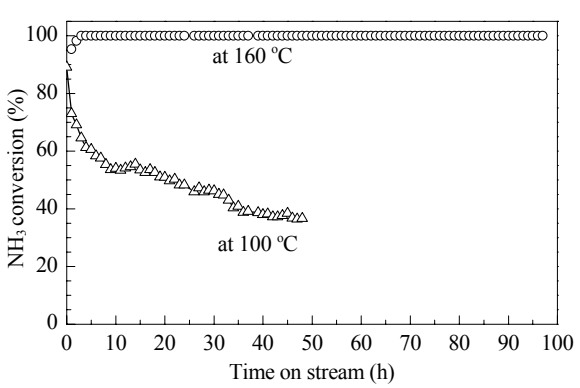

Fig. 2. Stability test of the H_2-pretreated $Ag_{0.1}Ce_{0.1}/Al_2O_3$ catalyst at various temperatures. Reaction conditions: NH_3 0.05 vol%, O_2 10 vol%, N_2 as balance, flow rate 200 cm^3/min, catalyst 0.2 g (W/F = 0.06 (g·s)/cm^3).

The performance of $Ag_{0.1}Ce_{0.1}/Al_2O_3$ was also compared with the reported results from Ag/Al_2O_3 and other noble metal catalysts [7]. The performance of $Ag_{0.1}Ce_{0.1}/Al_2O_3$

was superior to that of the Ag/Al_2O_3 and other noble catalysts at low temperatures and its N_2 selectivity (about 50% at temperatures below 160 °C) was similar to that of Ag/Al_2O_3. N_2O was the main by-product over $Ag_{0.1}Ce_{0.1}/Al_2O_3$ at low temperatures. With further improvement, this catalyst would be promising as a suitable catalyst at low temperatures (≤ 160 °C).

2.2 Characterization results

2.2.1 N_2 physisorption

The effects of CeO_2 addition on the textural characteristics of the co-impregnated Ag/Al_2O_3 samples were assessed by measuring N_2 adsorption-desorption isotherms. The results are shown in Table 1. The BET surface area, pore size, and pore volume of the Ce-promoted Ag/Al_2O_3 catalysts decreased with increasing Ce/Al_2O_3 ratio. At lower Ce loadings, the decrease in pore size can be attributed to the blockage by Ce species formed from excess Ce. At higher Ce loadings, this could be due to the smaller pores of CeO_2 deposited on the Al_2O_3 surface. The results showed that the activities of the $Ag_{0.1}Ce_y/Al_2O_3$ catalysts at low temperatures (Fig. 1) were not related to their BET surface areas.

Table 1 BET surface area and pore size of $Ag_{0.1}Ce_yAl_2O_3$ catalysts with different Ce/Al_2O_3 mass ratios

Sample	Surface area (m^2/g)	Pore volume (cm^3/g)	Average pore diameter (nm)
Al_2O_3	250	0.81	13.0
$Ag_{0.1}Ce_0/Al_2O_3$	249	0.80	12.9
$Ag_{0.1}Ce_{0.05}/Al_2O_3$	205	0.65	12.7
$Ag_{0.1}Ce_{0.1}/Al_2O_3$	206	0.63	12.2
$Ag_{0.1}Ce_{0.15}/Al_2O_3$	197	0.53	10.8
$Ag_{0.1}Ce_{0.2}/Al_2O_3$	173	0.52	12.0
$Ag_{0.1}Ce_{0.3}/Al_2O_3$	168	0.42	10.1

2.2.2 XRD

The XRD patterns of the $Ag_{0.1}Ce_y/Al_2O_3$ catalysts are shown in Fig. 3. In the unpromoted Ag/Al_2O_3, γ-Al_2O_3 was the only phase. With the Ce-promoted samples, diffraction lines from CeO_2 were present in addition to those of γ-Al_2O_3. The intensities of the CeO_2 lines became stronger and sharper with increasing Ce loading, demonstrating that the size of the CeO_2 particles on the γ-Al_2O_3 matrix increased with increasing Ce loading leading to a decrease in CeO_2 dispersion. This coincided with the decrease in BET surface area (Table 1). As shown in Fig. 1, the activity of the $Ag_{0.1}Ce_y/Al_2O_3$ catalyst at low temperatures first increased with increasing Ce loading ($y \le 0.1$), then decreased at higher loadings. This implied that a suitable Ce loading ($y \le 0.1$) gave the best dispersion of CeO_2 in $Ag_{0.1}Ce_y/Al_2O_3$, which gave the highest NH_3 conversion at low temperatures. Conversely, the reduced dispersion of CeO_2 at higher Ce loadings ($y > 0.1$) was one cause for the decrease in NH_3 oxidation activity over the $Ag_{0.1}Ce_y/Al_2O_3$ catalysts at temperatures below 160 °C.

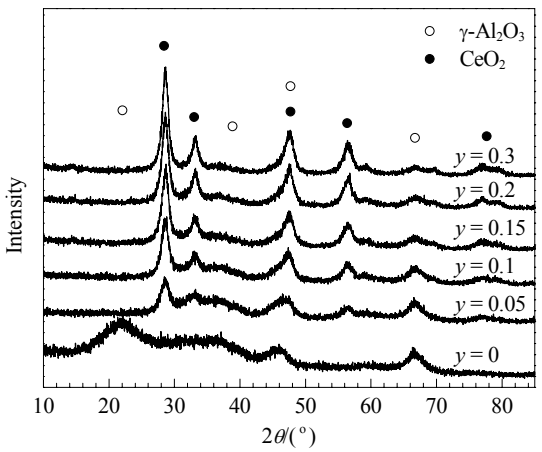

Fig. 3. XRD patterns of the fresh $Ag_{0.1}Ce_y/Al_2O_3$ catalysts with different Ce/Al_2O_3 mass ratios.

2.2.3 XPS

XPS was used to determine the element compositions and their chemical valences on the surfaces of fresh, H_2-pretreated $Ag_{0.1}Ce_{0.1}/Al_2O_3$ catalysts and the samples after the stability test. The results for Ag are not shown here, but previous data [4] indicated that the binding energies of the 3*d* electrons in Ag^0, Ag^+, or Ag^{2+} were similar. Therefore, it was difficult to get the oxidation state of the Ag species from the XPS results. Instead, these were obtained from UV-Vis DRS results.

The experimental and fitted Ce 3*d* spectra of the catalysts are shown in Fig. 4. The broad line for the Ce 3*d* core level indicated that both Ce^{3+} and Ce^{4+} existed. The curves were fitted with eight peaks, which corresponded to the four pairs of spin-orbit doublets [19–21]. The letters V and U refer to the Ce $3d_{5/2}$ and Ce $3d_{3/2}$ spin-orbit components, respectively. The relative percentage of the two Ce species was obtained from the area ratio of the Ce^{4+} $3d_{5/2}$ (V, V", V"') relative to Ce^{3+} $3d_{5/2}$ (V').

Table 2 shows the results of the XPS quantitative analysis based on the atomic ratios obtained. The chemical valence of Ce on the surface of fresh $Ag_{0.1}Ce_{0.1}/Al_2O_3$ was mainly Ce^{4+} with a small Ce^{3+} component. The surface ratio of Ce^{4+}/Ce^{3+} on fresh $Ag_{0.1}Ce_{0.1}/Al_2O_3$ decreased with H_2-pretreatment, with some surface Ce^{4+} reduced to Ce^{3+}. The surface ratio of Ce^{4+}/Ce^{3+} increased during the stability test at 100 °C for 48 h (4.6), which indicated that some Ce^{3+}

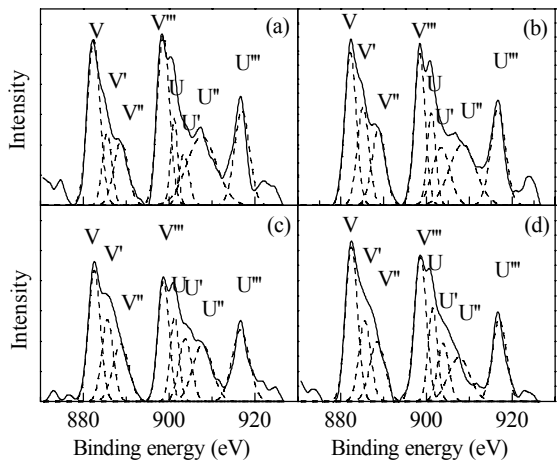

Fig. 4. Experimental and fitted Ce 3*d* XPS profiles for $Ag_{0.1}Ce_{0.1}/Al_2O_3$ catalysts: (a) H_2-pretreated; (b) Kept at 100 °C for 48 h; (c) Kept at 160 °C for 96 h; (d) Fresh catalyst.

was gradually oxidized at 100 °C over 48 h. In addition, the surface ratio of Ce^{4+}/Ce^{3+} increased further after testing at 160 °C for 96 h (5.2), which demonstrated that more Ce^{3+} was oxidized at the higher temperature with the longer period of time. Taking into account this and the activity test results shown in Fig. 2, it can be seen that while NH_3 conversion at 100 °C decreased gradually together with the partial oxidation of Ce^{3+} in which Ce^{4+}/Ce^{3+} was increased to 4.6, the conversion did not decrease at the higher temperature of 160 °C despite more partial oxidation of Ce^{3+} in which Ce^{4+}/Ce^{3+} was increased to 5.2.

Table 2 XPS data (Ce^{4+}/Ce^{3+}) from the $Ag_{0.1}Ce_{0.1}/Al_2O_3$ catalysts in Fig. 4

$Ag_{0.1}Ce_{0.1}/Al_2O_3$ catalyst	Ce^{4+}/Ce^{3+}
H_2-pretreated	4.4
Retained at 100 °C for 48 h	4.6
Retained at 160 °C for 96 h	5.2
Fresh	6.3

2.2.4 UV-Vis DRS

The results of the UV-Vis DRS confirmed the details of the state of the supported Ag and Ce species. Fig. 5 shows the UV-Vis DRS of the fresh, H_2-pretreated $Ag_{0.1}Ce_{0.1}/Al_2O_3$ catalyst and two samples after stability test as described above. The UV-Vis DRS analysis demonstrated the existence of different states of the Ag and Ce species, which can be seen after subtraction of the Al_2O_3 spectrum. Fresh $Ag_{0.1}Ce_{0.1}/Al_2O_3$ showed broad absorption bands at 206, 220, 260, and 305 nm, while the other three samples had an additional broad band at 450 nm (Fig. 5(a)). The bands at 206, 450, and 260 nm can be attributed to highly dispersed Ag^+ ions, metallic silver (Ag^0) particles

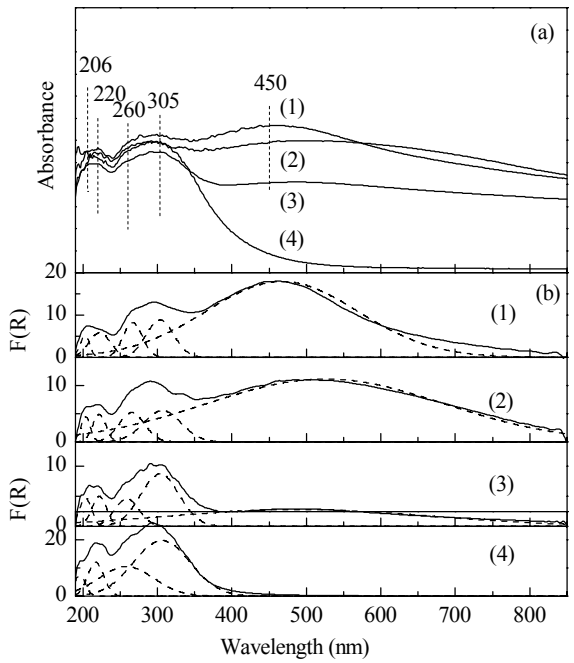

Fig. 5. Diffuse reflectance UV-Vis spectra (a) and deconvoluted subbands (b) of the $Ag_{0.1}Ce_{0.1}/Al_2O_3$ catalysts. (1) H_2-pretreated; (2) Retained at 100 °C for 48 h; (3) Retained at 160 °C for 96 h; (4) Fresh catalyst.

[9–15], and Ce^{3+} [17,18], respectively. The bands at 220 and 305 nm can be attributed to Ce^{4+} [16–18].

In Fig. 5(b), the measured spectra of the $Ag_{0.1}Ce_{0.1}/Al_2O_3$ catalysts have been treated by Kubelka-Munk functions and deconvoluted into Gaussian peaks assigned to different Ag and Ce species [9–18]. Deconvolution was performed based on the above assignments. The relative intensities of these peaks are listed in Table 3, along with the quantification results for the different Ag and Ce species: I_1 for Ag^+ (band at $\lambda < 238$ nm), I_2 for Ag^0 ($\lambda > 350$ nm), I_3 for Ce^{3+} (250 nm $< \lambda <$ 300 nm), and I_4 for Ce^{4+} (210 nm $< \lambda <$ 250 nm and 260 nm $< \lambda <$ 350 nm). Although the peaks can be used to give a semi-quantitative description of the distribution of the different species, the quantification results shown in Table 3 provides a better comparison of the relative amounts of the various Ag and Ce species on the catalysts.

Table 3 Percentage of integrated area of the peaks derived from deconvolution of the UV-Vis DRS in Fig. 5

$Ag_{0.1}Ce_{0.1}/Al_2O_3$ catalyst	I_1[a]/%	I_2[b]/%	I_3[c]/%	I_4[d]/%
Fresh	100	0	12.5	87.5
H_2-pretreated	1.8	98.2	27.6	72.4
Retained at 100 °C for 48 h	2.0	98.0	23.3	77.7
Retained at 160 °C for 96 h	7.3	92.7	21.5	78.5

[a]For Ag^+ (band at $\lambda < 238$ nm).

[b]For Ag^0 (band at $\lambda > 350$ nm).

[c]For Ce^{3+} (band at 250 nm $< \lambda <$ 300 nm).

[d]For Ce^{4+} (band at 210 $< \lambda <$ 250 nm and 260 $< \lambda <$ 350 nm).

The UV-Vis DRS results (Fig. 5) also confirmed that Ce^{3+} and Ce^{4+} coexisted on the alumina support. Furthermore, the relative amount of Ce^{4+} decreased following H_2-pretreatment but increased slightly following the stability test for 48 h at 100 °C and then increased more significantly after the stability test for 96 h at 160 °C. This was in agreement with the XPS results (Table 2). It can be concluded that some Ce^{3+} on the surface of the H_2-pretreated $Ag_{0.1}Ce_{0.1}/Al_2O_3$ catalyst was oxidized to Ce^{4+} at both 100 and 160 °C during the stability test, but the relative amounts of Ce^{4+} were lower than that in the fresh catalyst.

In fresh $Ag_{0.1}Ce_{0.1}/Al_2O_3$, Ag^+ was the major Ag species present. On the H_2-pretreated catalyst, Ag^0 was the main Ag species present (Table 3), showing that most Ag_xO on the support was reduced to Ag^0 by the H_2-pretreatment. Taken together with the activity test results shown in Fig. 1, this showed that high NH_3 conversion was obtained over the H_2-pretreated $Ag_{0.1}Ce_{0.1}/Al_2O_3$ catalyst in the temperature range of 100–160 °C with the presence of Ag^0, while almost no NH_3 conversion was observed over the H_2-pretreated $Ce_{0.1}/Al_2O_3$ or fresh $Ag_{0.1}Ce_{0.1}/Al_2O_3$ due to the absence of Ag^0. That is, the presence of Ag^0 explains the enhanced low temperature activity of the H_2-pretreated $Ag_{0.1}Ce_{0.1}/Al_2O_3$ catalyst. It can therefore be concluded that Ag^0 is the main active species on this catalyst that is responsible for NH_3 oxidation at temperatures below 160 °C. However, a comparison with the H_2-pretreated $Ag_{0.1}/Al_2O_3$ catalyst showed the H_2-pretreated $Ag_{0.1}Ce_{0.1}/Al_2O_3$ catalyst has a much higher NH_3 conversion in the presence of Ce. This showed that Ce has an important role in NH_3 oxidation at low temperature. This will be discussed in detail in the following section.

It was also found that Ag^0 was slightly oxidized after the stability test for more than 48 h at 100 °C while some Ce^{3+} on the surface of the catalyst was oxidized to Ce^{4+} under the same conditions. During this time, NH_3 conversion decreased gradually (Fig. 2). Consequently, Ce^{3+} oxidation can partly explain the decrease in catalytic activity at 100 °C with H_2-pretreated $Ag_{0.1}Ce_{0.1}/Al_2O_3$.

It is worth noting that both Ag^0 and Ce^{3+} were partly oxidized during the stability test at 160 °C for 96 h (Fig. 5), but that 100% NH_3 conversion was maintained throughout (Fig. 2).

2.2.5 HR-TEM

The HR-TEM images shown in Fig. 6 for the H_2-pretreated $Ag_{0.1}/Al_2O_3$ and $Ag_{0.1}Ce_{0.1}/Al_2O_3$ catalysts show the surface distribution of Ag particles. Statistical calculations of Ag particle size measured from these images provided the mean particle size (d) and degree of Ag dispersion (Table 4). The particles were assumed to be spherical.

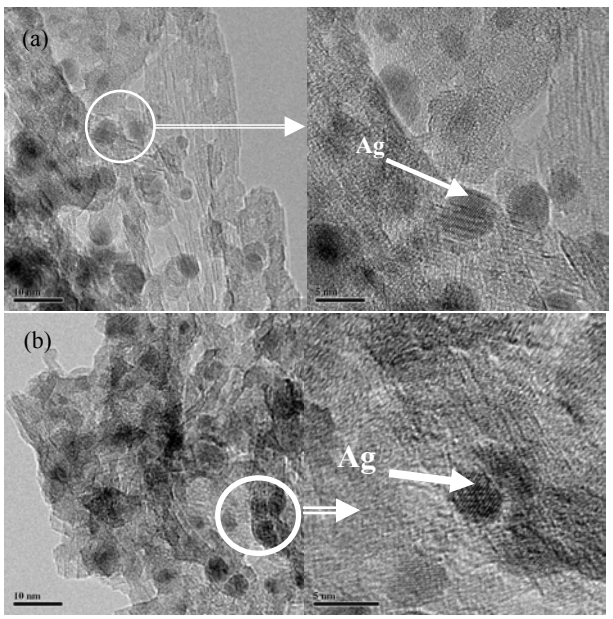

Fig. 6. HR-TEM images of the H_2-pretreated $Ag_{0.1}/Al_2O_3$ (a) and $Ag_{0.1}Ce_{0.1}/Al_2O_3$ (b) catalysts.

Table 4 Ag dispersion (D), mean particle size (d), and turnover frequency (TOF) of H_2-pretreated $Ag_{0.1}/Al_2O_3$ and $Ag_{0.1}Ce_{0.1}/Al_2O_3$ catalysts at 100 °C

Catalyst	d^a/nm	D^b/%	TOF^c (10^{-3}/s)
$Ag_{0.1}/Al_2O_3$	4.6	29.0	0.36
$Ag_{0.1}Ce_{0.1}/Al_2O_3$	5.2	25.5	1.61

Reaction conditions: catalyst 0.2 g, NH_3 0.05 vol%, O_2 10 vol%, total flow rates 200 cm^3/min, temperature 100 °C.

[a]Determined by HR-TEM.

[b]Spherical Ag crystallites are assumed, and the relationship between crystallite diameter size (d) and dispersion D is $d = 1.34/D$ [22].

[c]Calculated as moles of NH_3 converted per mole of Ag on the whole catalyst per second.

The relationship between the crystallite diameter (d) and Ag dispersion (D) was $d = 1.34/D$ [22]. H_2-pretreated $Ag_{0.1}Ce_{0.1}/Al_2O_3$ had a Ag mean particle size of 5.2 nm, which is similar to that of $Ag_{0.1}/Al_2O_3$ (4.6 nm). This is consistent with the previous results based on O_2 chemisorption [7]. The Ag dispersion had to be determined by HR-TEM based on a H_2-pretreated $Ag_{0.1}Ce_{0.1}/Al_2O_3$ catalyst because reduced CeO_x chemisorbs O_2.

It was found that Ag^0 was the main active species involved in NH_3 oxidation in H_2-pretreated $Ag_{0.1}Ce_{0.1}/Al_2O_3$ at temperatures below 160 °C, which was in agreement with previous results on H_2-pretreated Ag/Al_2O_3 [7]. The HR-TEM images from the present study showed that H_2-pretreated $Ag_{0.1}Ce_{0.1}/Al_2O_3$ and $Ag_{0.1}/Al_2O_3$ both had similar Ag dispersions. The turnover frequency (TOF) for NH_3 at 100 °C (Table 4), however, showed that $Ag_{0.1}Ce_{0.1}/Al_2O_3$ had a better activity than $Ag_{0.1}/Al_2O_3$.

These results indicated that Ag dispersion is not the primary contribution to the difference in activity observed between these two samples at low temperature. Indeed, the enhanced activity at low temperatures may be primarily linked to the role of the Ce species.

2.3 In situ DRIFTS study of NH_3 adsorption

In order to investigate the role of Ce and Ag for the adsorption of NH_3 on the catalysts, in situ DRIFTS spectra for the H_2-pretreated $Ce_{0.1}/Al_2O_3$ and $Ag_{0.1}Ce_{0.1}/Al_2O_3$ catalysts exposed to NH_3 are shown in Fig. 7. In Fig. 7(a), the bands at 1695, 1481, and 1392 cm^{-1} are from the deformation modes of NH_4^+ formed by the interaction of NH_3 with Brönsted acid sites on γ-Al_2O_3 [2,23–27]. The bands at 1608 and 1240 cm^{-1} can be attributed to the asymmetric and symmetric deformation modes, respectively, of NH_3 molecules coordinated on Lewis acid sites of the γ-Al_2O_3 [23–27]. The band at 1456 cm^{-1} can be attributed to imide (–NH) deformation modes [2,28,29]. The two shoulders at 1580 and 1376 cm^{-1} can be assigned to amide ($–NH_2$) scissoring and ($–NH_2$) wagging, respectively [2,28,29]. The bands in the N–H stretching region also occur at 3401, 3356, 3270, and 3149 cm^{-1} [28,29].

The band intensities from NH_3 coordinated on Brönsted (1695, 1481, and 1392 cm^{-1}) and Lewis acid sites (1608 and 1240 cm^{-1}) decreased gradually with increasing temperature. Those related to $–NH_2$ and –NH (1580, 1456, and 1376 cm^{-1}) appeared at room temperature together with those of NH_3, but disappeared at higher temperatures (Fig. 7(a)). These results showed that NH_3 adsorbed on H_2-pretreated $Ce_{0.1}/Al_2O_3$ was adsorbed dissociatively to form $–NH_2$ and –NH intermediates and followed reactions (1) and (2) with the abstraction of hydrogen. Furthermore, these $–NH_2$ and –NH are stable on H_2-pretreated $Ce_{0.1}/Al_2O_3$ and do not disappear until a temperature of 400 °C.

$$NH_3 \rightarrow NH_2 + H \quad (1)$$

$$NH_2 \rightarrow NH + H \quad (2)$$

In the case of the H_2-pretreated $Ag_{0.1}Ce_{0.1}/Al_2O_3$ catalyst, similar bands occurred at 1695, 1608, 1481, 1456, 1392, 1365, and 1240 cm^{-1} following NH_3 adsorption (Fig. 7(b)). The bands of NH_3 adsorbed on the Brönsted and Lewis acid sites of $Ag_{0.1}Ce_{0.1}/Al_2O_3$ disappeared at 160 °C. While the intensity of these bands decreased with increasing temperature, the bands corresponding to $–NH_2$ (1365 cm^{-1}) and –NH (1456 cm^{-1}) increased and then disappeared at temperatures below 160 °C, indicating that NH_3 adsorbed on H_2-pretreated $Ag_{0.1}Ce_{0.1}/Al_2O_3$ was activated to form $–NH_2$ and –NH intermediates first and then desorbed from the surface of the catalyst. Comparing with the in situ DRIFTS results in Fig. 7(a), it is seen that the adsorbed NH_3 on both H_2-pretreated $Ag_{0.1}Ce_{0.1}/Al_2O_3$ and $Ce_{0.1}/Al_2O_3$ can be activated to form $–NH_2$ and –NH intermediates, but the $–NH_2$ and –NH formed can be activated and desorbed from the surface of H_2-pretreated $Ag_{0.1}Ce_{0.1}/Al_2O_3$ much faster in the presence of Ag^0. In addition, according to our previous in situ DRIFTS results of NH_3 adsorption on H_2-pretreated $Ag_{0.1}/Al_2O_3$ [30], bands corresponding to $–NH_2$ and –NH did not appear at room temperature, which is different from that with H_2-pretreated $Ce_{0.1}/Al_2O_3$. Hence, we conclude that CeO_2 addition promoted the dissociative adsorption of NH_3 to form $–NH_2$ and –NH intermediates.

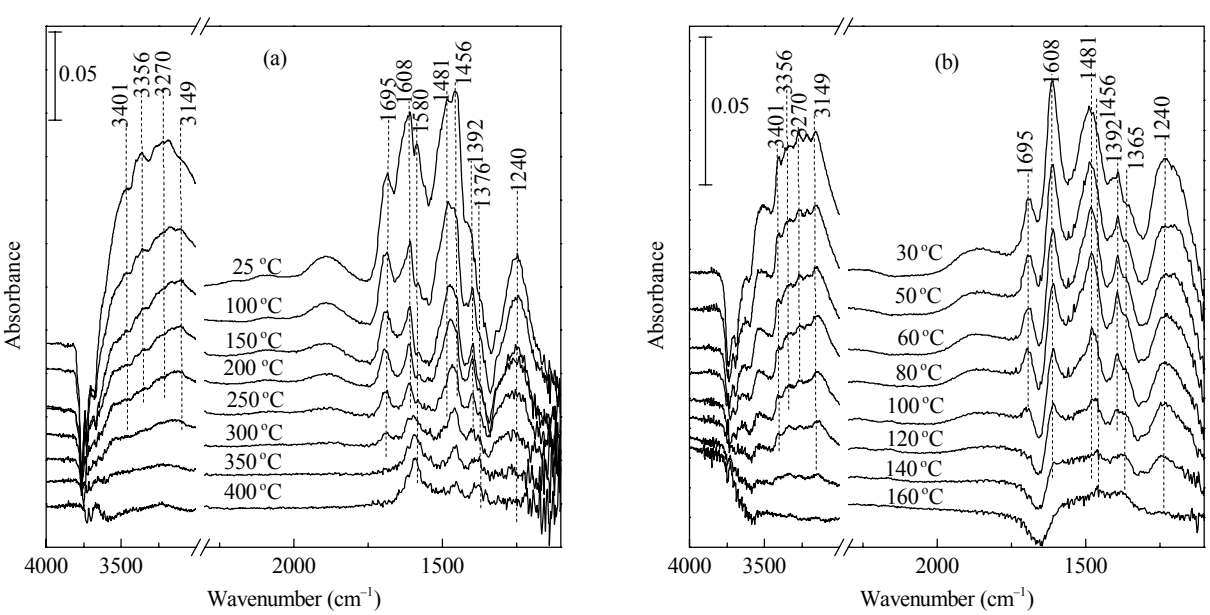

Fig.7. In situ DRIFTS spectra of the adsorbed species arising from contact of NH_3 (0.05 vol%) with the H_2-pretreated $Ce_{0.1}/Al_2O_3$ (a) and $Ag_{0.1}Ce_{0.1}/Al_2O_3$ (b) at room temperature and successive purging with N_2 at various temperatures.

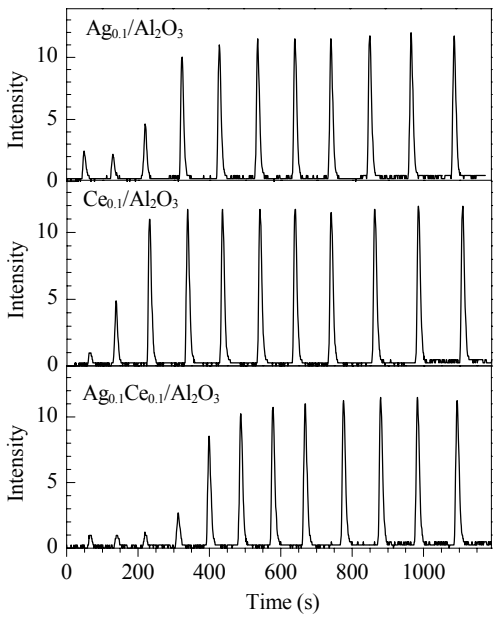

Fig. 8. O_2 uptakes on the H_2-pretreated $Ag_{0.1}/Al_2O_3$, $Ce_{0.1}/Al_2O_3$, and $Ag_{0.1}Ce_{0.1}/Al_2O_3$ catalysts at 100 °C.

2.4 O_2-pulse adsorption

The O_2 uptakes of the catalysts were determined by measuring O_2-pulse adsorption at 100 °C. As shown in Fig. 8, O_2 was chemisorbed on the three catalysts. As expected, the amount of O_2 uptake on $Ag_{0.1}Ce_{0.1}/Al_2O_3$ (69.71 μmol/g) was much higher than that on either $Ag_{0.1}/Al_2O_3$ (45.73 μmol/g) or $Ce_{0.1}/Al_2O_3$ (36.47 μmol/g).

Gang et al. [6,8] reported on adsorbed atomic oxygen (O) on reduced Ag catalysts, and considered the dissociation of O_2 to be the rate controlling step in NH_3 oxidation [8]. Lefferts et al. [31] also detected O on a H_2-pretreated Ag surface. From the present O_2-pulse adsorption results, it is likely that some molecular O_2 was chemisorbed dissociatively on the surface of H_2-pretreated $Ag_{0.1}/Al_2O_3$ as O species.

Li et al. [32] reported that molecular O_2 was adsorbed on the surface of partially reduced cerium oxide to form a superoxide species (O_2^-), which can be further chemisorbed dissociatively to O on the surface of H_2-reduced cerium oxide. In the present study, some surface Ce^{4+} of the H_2-pretreated $Ag_{0.1}Ce_{0.1}/Al_2O_3$ was reduced to Ce^{3+} by H_2 reduction (Tables 2 and 3). This can lead to the formation of surface oxygen nests together with bulk oxygen vacancies, to result in the dissociative adsorption of O_2 on reduced cerium oxide. Taken together with the O_2 pulse-adsorption results (Fig. 8), it can be concluded that some molecular O_2 is chemisorbed dissociatively to form O on the surface of H_2-pretreated $Ce_{0.1}/Al_2O_3$, which would explain the enhanced O_2 uptake on the H_2-pretreated $Ag_{0.1}Ce_{0.1}/Al_2O_3$ catalyst.

From these results, it can be concluded that adding CeO_2 enhanced the O_2 uptake of Ag/Al_2O_3 by promoting the catalytic ability of Ag/Al_2O_3 for dissociative or non-dissociative adsorption of O_2 at low temperatures (100 °C). The NH_3 oxidation activity of Ag/Al_2O_3 at low temperatures is determined by its catalytic ability for both dissociative and non-dissociative adsorption of O_2 [6]. Chemisorbed O enhanced NH_3 oxidation below 140 °C on Ag/Al_2O_3, while gas phase molecular O_2 mainly interacted with adsorbed NH_3 at temperatures above 140 °C [30]. From Fig. 1 it can be seen that higher NH_3 conversion occurred on H_2-pretreated $Ag_{0.1}Ce_{0.1}/Al_2O_3$, with a higher O_2 uptake at 100 °C. This confirmed that O_2 uptake was the main factor causing the enhanced low temperature activity of the catalyst, since the addition of CeO_2 improved the activation of O_2 to form O at 100 °C. In addition, our previously reported results [30] showed that O favors the activation of adsorbed NH_3 to form –NH and –HNO intermediates (reactions (3)–(5)), which are the key intermediates for NH_3 oxidation (route (6) and (7)) at low temperatures (< 140 °C).

$$NH_3 + O \rightarrow NH + H_2O \quad (3)$$

$$O_2 \rightarrow 2O \quad (4)$$

$$NH + O \rightarrow HNO \quad (5)$$

$$NH + HNO \rightarrow N_2 + H_2O \quad (6)$$

$$HNO + HNO \rightarrow N_2O + H_2O \quad (7)$$

Hence, we conclude that adding CeO_2 to Ag/Al_2O_3 improved the catalyst's ability in the adsorption and activation of O_2 to form O. Then the O species activated adsorbed NH_3 to form –NH and –HNO intermediates. Our in situ DRIFTS results also proved that adding CeO_2 favored the dissociative adsorption of NH_3 to form $–NH_2$ and –NH (reactions (1) and (2)), giving the reason for the enhanced activity of the H_2-pretreated $Ag_{0.1}Ce_{0.1}/Al_2O_3$ at temperatures below 160 °C.

The 100 °C/48 h stability test results (Fig. 2) showed that the high degree of NH_3 conversion decreased gradually with the oxidation of some Ce^{3+} (Tables 2 and 3), although Ag^0 showed little oxidation under these conditions. This presumably reflected a decrease in the ability of the catalyst to participate in the dissociative adsorption of O_2 as a result of the oxidation of Ce^{3+}, thus contributing to a decrease in NH_3 oxidation activity at 100 °C.

The 160 °C/96 h stability test results, however, showed that 100% NH_3 conversion was maintained throughout (Fig. 2), although both Ag^0 and Ce^{3+} were partly oxidized during the test (Fig. 5). Gas phase molecular O_2 mainly interacted with adsorbed NH_3 at temperatures above 140 °C on Ag/Al_2O_3 [30]. Hence, it can be inferred that at the higher temperature of 160 °C, adsorbed NH_3 mainly interacted with O_2 on $Ag_{0.1}Ce_{0.1}/Al_2O_3$ and any partial oxidation of Ce^{3+} did not affect the activity under these conditions. Furthermore,

Ag^+ is the active species on Ag/Al_2O_3 at temperatures above 140 °C [7], and thus Ag^+ on $Ag_{0.1}Ce_{0.1}/Al_2O_3$ is likely also the active species involved in NH_3 oxidation at 160 °C. Hence, high NH_3 conversion will persist in spite of the oxidation of some Ag^0 species.

3 Conclusions

The addition of an appropriate amount of CeO_2 to Ag/Al_2O_3 improved the catalytic oxidation of NH_3 at temperatures below 160 °C. Ag^0 is the main active species on a H_2-pretreated $Ag_{0.1}Ce_y/Al_2O_3$ catalyst. It is responsible for the adsorption and activation of NH_3 and O_2 simultaneously at temperatures below 160 °C. The addition of CeO_2 enhanced the catalyst's ability to adsorb and activate O_2 to O, the O to further activate adsorbed NH_3, and also the dissociative adsorption of NH_3. This was the main reason for the enhancement of NH_3 oxidation at low temperatures (≤ 160 °C) over $Ag_{0.1}Ce_{0.1}/Al_2O_3$.

References

1 Gang L, Anderson B G, van Grondelle J, van Santen R A. *Catal Today*, 2000, **61**: 179
2 Lin S D, Gluhoi A C, Nieuwenhuys B E. *Catal Today*, 2004, **90**: 3
3 Lippits M J, Gluhoi A C, Nieuwenhuys B E. *Catal Today*, 2008, **137**: 446
4 Gang L, Anderson B G, van Grondelle J, van Santen R A, van Gennip W J H, Niemantsverdriet J W, Kooyman P J, Knoester A, Brongersma H H. *J Catal*, 2002, **206**: 60
5 贺泓, 余运波, 李毅, 吴强, 张秀丽, 张长斌, 石晓燕, 宋小萍. 催化学报 (He H, Yu Y B, Li Y, Wu Q, Zhang X L, Zhang Ch B, Shi X Y, Song X P. *Chin J Catal*), 2010, **31**: 491
6 Gang L, Anderson B G, van Grondelle J, van Santen R A. *Appl Catal B*, 2003, **40**: 101
7 Zhang L, Zhang C, He H. *J Catal*, 2009, **261**: 101
8 Gang L, Anderson B G, van Grondelle J, van Santen R A. *J Catal*, 2001, **199**: 107
9 Bogdanchikova N, Meunier F C, Avalos-Borja M, Breen J P, Pestryakov A. *Appl Catal B*, 2002, **36**: 287
10 Sato K, Yoshinari T, Kintaichi Y, Haneda M, Hamada H. *Appl Catal B*, 2003, **44**: 67
11 Keshavaraja A, She X, Flytzani-Stephanopoulos M. *Appl Catal B*, 2000, **27**: L1
12 She X, Flytzani-Stephanopoulos M. *J Catal*, 2006, **237**: 79
13 Shimizu K, Tsuzuki M, Kato K, Yokota S, Okumura K, Satsuma A. *J Phys Chem C*, 2007, **111**: 950
14 Hoost T E, Kudla R J, Collins K M, Chattha M S. *Appl Catal B*, 1997, **13**: 59
15 Kundakovic L, Flytzani-Stephanopoulos M. *Appl Catal A*, 1999, **183**: 35
16 Bensalem A, Bozon-Verduraz F, Delamar M, Bugli G. *Appl Catal A*, 1995, **121**: 81
17 Si R, Zhang Y W, Li S J, Lin B X, Yan C H. *J Phys Chem B*, 2004, **108**: 12481
18 Timofeeva M N, Jhung S H, Hwang Y K, Kim D K, Panchenko V N, Melgunov M S, Chesalov Y A, Chang J S. *Appl Catal A*, 2007, **317**: 1
19 Ferriz R M, Gorte R J, Vohs J M. *Catal Lett*, 2002, **82**: 123
20 Liotta L F, Carlo G D, Pantaleo G, Venezia A M, Deganello G. *Appl Catal B*, 2006, **66**: 217
21 Zhao M, Shen M, Wen X, Wang J. *J Alloy Compd*, 2008, **457**: 578
22 Lu J, Bravo-Suárez J J, Haruta M, Oyama S T. *Appl Catal A*, 2006, **302**: 283
23 Amblard M, Burch R, Southward B W L. *Catal Today*, 2000, **59**: 365
24 Larrubia M A, Ramis G, Busca G. *Appl Catal B*, 2001, **30**: 101
25 Ramis G, Larrubia M A, Busca G. *Top Catal*, 2000, **11**: 161
26 Kijlstra W S, Brands D S, Poels E K, Bliek A. *J Catal*, 1997, **171**: 208
27 Zou H, Shen J. *Thermochim Acta*, 2000, **351**: 165
28 Amores J M G, Escribano V S, Ramis G, Busca G. *Appl Catal B*, 1997, **13**: 45
29 Ramis G, Yi L, Busca G, Turco M, Kotur E, Willey R J. *J Catal*, 1995, **157**: 523
30 Zhang L, He H. *J Catal*, 2009, **268**: 18
31 Lefferts L, van Ommen J G, Ross J R H. *Appl Catal*, 1987, **31**: 291
32 Li C, Domen K, Maruya K, Onishi T. *J Am Chem Soc*, 1989, **111**: 7683